

# Population Gradients in Galaxy Clusters at $0.2 < z < 0.6$

E. Ellingson

*Center for Astrophysics and Space Astronomy, Univ. of Colorado,  
Boulder, CO, 80309*

H. Lin

*Steward Observatory, Univ. of Arizona, Tucson, AZ, 85721*

H.K.C. Yee and R. G. Carlberg

*Dept. of Astronomy, Univ. of Toronto, Toronto, Ontario, M5S 3H8,  
Canada*

**Abstract.** We present a principal component analysis of galaxy spectra from the CNOC sample of rich X-ray luminous clusters at  $0.18 < z < 0.55$ . Composite radial distributions of different stellar populations show strong gradients as a function of cluster-centric redshift. The composite population is dominated by evolved populations in the core, and gradually changes to one which is similar to coeval field galaxies at radii greater than the virial radius. We do not see evidence in the clusters for an excess of star formation over that seen in the coeval field. Within this redshift range, significant evolution in the gradient shape is seen, with higher redshift clusters showing steeper gradients. This results in larger numbers of younger galaxies seen towards the inner regions of the clusters— in effect, a restatement of the Butcher-Oemler effect. Luminosity density profiles are consistent with a scenario where this phenomenon is due to a decline over time in the infall rate of field galaxies into clusters. Depending on how long galaxies reside in clusters before their star formation rates are diminished, this suggests an epoch for maximal infall into clusters at  $z > 0.7$ . We also discuss alternative scenarios for the evolution of cluster populations.

## 1. Introduction

The evolving populations in galaxy clusters offer a unique opportunity to observe galaxy evolution in action, and particularly the effects of environment on star forming galaxies. Present-day rich clusters have strikingly different populations from galaxies in poorer environments, suggesting that some mechanism is at work transforming normal field galaxies into the cluster population. Many recent investigations have focused on the details of how this transformation occurs (Couch & Sharples 1987, Barger et al., 1996, Poggianti et al., 1999, Balogh et al., 1999). The emerging picture is that there may be a population of galax-

ies which were formed very early in the cluster's history, corresponding to the ellipticals often seen in cluster cores. (e.g. Bower et al., 1992, Ellis et al., 1997) Subsequent generations of infalling field galaxies have had their star formation disrupted, possibly with an associated starburst. As this transformation progresses, these galaxies might be identified with normal-looking spirals, then galaxies with strong Balmer absorption spectra, and finally S0 galaxies which have retained some of their disk structure but have ceased active star formation.

Most of these insights have been obtained by observing distant clusters, as higher redshift clusters have been shown to contain a higher fraction of star-forming galaxies—first described as the Butcher-Oemler effect (Butcher & Oemler 1984). Ostensibly, the processes which create present day clusters are at an earlier stage of their work at these epochs, and these clusters provide a time sequence for observing the growth of the cluster structure. Here we describe an investigation into the relationship between galaxy evolution and cluster structure, based on a well-defined and fairly homogeneous sample of intermediate redshift clusters, and coeval field galaxy measurements. In an approach complementary to that of looking at galaxy properties in detail, we instead focus on building smooth composite spatial distributions within the cluster of the various stellar populations. With these distributions, it is possible to chart the relationship between the evolution of galaxy populations and the growth and evolution of the cluster.

## 2. The CNOC Cluster Sample

The CNOC (Canadian Network for Observational Cosmology) Cluster Redshift Survey targeted 16 rich X-ray luminous galaxy clusters with  $0.17 < z < 0.55$ . Deep Gunn  $g$  and  $r$  imaging and multi-slit spectroscopic observations from the Canada-France-Hawaii 3.6m telescope were used to map the cluster sample to radii of  $1-3 h^{-1}$  Mpc from the cluster cores (see Yee et al., 1996). Wavelength coverage was  $\sim 3500 - 4500 \text{ \AA}$  in the rest frame of each cluster, with resolution of about  $15 \text{ \AA}$ . A total of 1200 cluster galaxies were spectroscopically identified. Particular care was taken to quantify selection effects and the completeness of the sample as a function of galaxy magnitude, color, redshift and position. The wide field coverage and careful attention to the empirical selection functions are crucial for building an accurate portrait of cluster structure.

Dynamical and spatial analyses of the clusters (Carlberg et al., 1996, Carlberg, Yee & Ellingson 1997, Carlberg et al., 1997a,b) yielded cluster masses, mass-to-light ratios and density profiles. Lewis et al., (1999) presented the X-ray gas profiles from ROSAT HRI and PSPC observations of much of the sample. Balogh et al., (1997, 1999) analyzed spectral line indices for cluster galaxies. Here we combine measurements of the stellar populations in the cluster galaxies with the dynamical and X-ray properties of the clusters to address the issue of galaxy evolution in terms of the spatial distribution of different populations.

## 3. Principal Component Analysis

Principal component analysis (PCA) provides a sensitive method for measuring the strengths of different stellar populations from spectroscopic data. This tech-

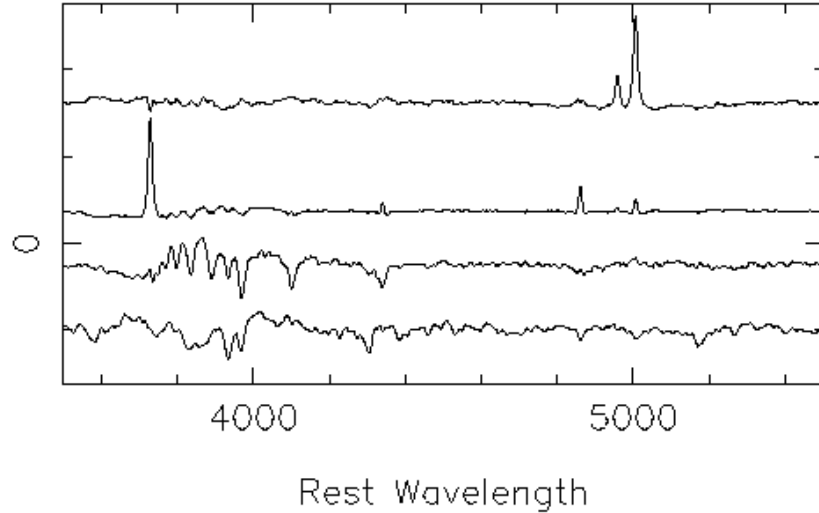


Figure 1. Principal Component Vectors derived from the Las Campanas Redshift Survey. Four vectors are defined: two which are combined to form our “Emission” vector, “Balmer,” and “Elliptical”.

nique has been used by other groups (e.g. Connolly et al., 1995, see also Zaritsky, Zabludoff & Willick 1995) to determine galaxy populations. It is especially applicable to the fairly noisy high-redshift data of the CNOC survey, because the entire spectrum, rather than a narrowly defined range of line indices, contributes to the measurement. We project each spectrum as the sum of four orthonormal galaxy “vectors.” These vectors are derived from relatively high quality galaxy spectra in the Las Campanas Redshift Survey (Shectman et al., 1996) at low redshift. Figure 1 shows the four original vectors, which correspond roughly to two “Emission line” components ([OII] and [OIII]), which we combine to a single vector because our spectra do not extend to the H- $\beta$ /[OIII] region), a “Balmer component” featuring strong Balmer absorption lines indicative of intermediate age stars, and an “Elliptical” spectrum showing the standard old-population features. The power in each of the three components provides a measurement of the stellar population.

The combination of these three PCA components are adequate to separate most types of normal galaxies. Figure 2 shows PCA components for galaxies in the Kennicutt Spectral Atlas of low redshift galaxies (Kennicutt, 1992). Normal elliptical and spiral galaxies are well separated on this plot. Note that the Kennicutt Atlas does not populate the region of the plot with large Balmer values and low emission line values. In this region we plot high signal-to-noise ratio examples of K+A galaxies from the CNOC clusters.

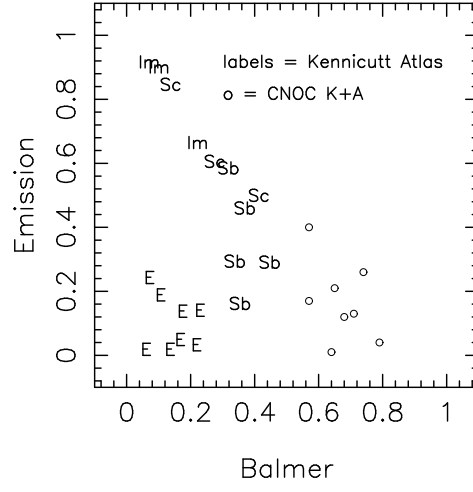


Figure 2. PCA Decomposition of Galaxies from the Kennicutt Spectral Atlas. Morphological types of the low redshift galaxies are labeled. Open circles denote K+A galaxies from the CNOC clusters. The normalization of the sum of the three components to 1 means that non-zero data occupy a triangular region on this plot.

#### 4. Population Gradients in Galaxy Clusters

A composite average population gradient from 15 clusters was constructed from galaxies with k-corrected  $M_r < -19$  ( $H_0 = 100 \text{ km s}^{-1} \text{ Mpc}^{-1}$ ,  $q_0 = 0.1$ ). Cluster membership was delineated by a redshift within 3 times the line-of-sight velocity dispersion from the mean redshift. Galaxy positions were scaled by a characteristic radius,  $r_{200}$ , determined for each cluster by Carlberg et al., (1996), to normalize for differing cluster richness, and so that values at a given  $r/r_{200}$  represent those at a fixed overdensity. Typically,  $r_{200} \sim 0.75\text{--}1.5 \text{ h}^{-1} \text{ Mpc}$  for these clusters, and virial radii are 1.5–2  $r_{200}$ . These dynamical parameters are well determined for these clusters by 30–200 cluster members each, and have been found to yield results consistent with X-ray determinations of the cluster masses (Lewis et al., 1999). The CNOC cluster MS0906+11 was omitted because it shows strong binary substructure in both X-ray and velocity data, and robust values for dynamical parameters were not possible.

Weights for each galaxy were calculated as inverses of the completeness functions for magnitude, color and position within each cluster field based on deep two-color galaxy photometry in the fields (see Yee et al., 1996 for details on completeness functions). Using weights such as these ensures that our spectroscopic sample yields a result representative of the entire cluster.

A clear spatial gradient is seen, with the elliptical-like population declining from the cluster core towards the outer parts of the cluster, and an accompanying increase in emission line galaxies (Figure 3). There are between 20 and 294 galaxies in each bin; uncertainties were estimated via bootstrap techniques. A self-consistent correction for projection effects was tested, assuming an average

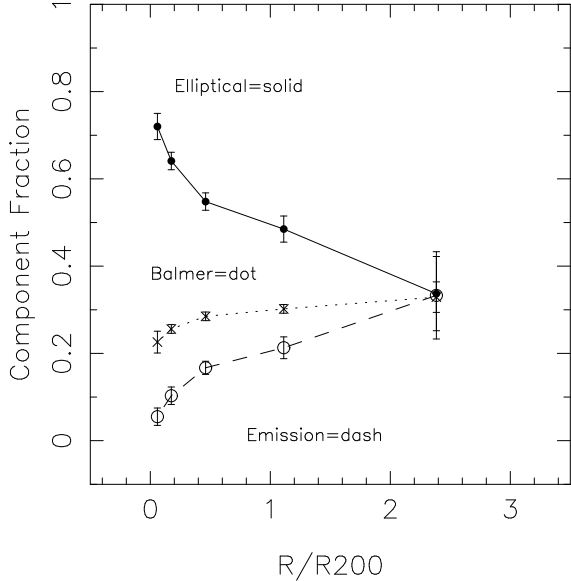


Figure 3. Composite radial gradients from 15 clusters based on the vectors shown in Figure 1. Normal field galaxies at these redshifts have values approximately equal to [0.30, 0.40, 0.30] for Elliptical, Emission and Balmer, respectively.

spherical galaxy distribution, but is not included in the figures shown here. This correction tends to steepen the gradient very slightly but is very small, generally raising the innermost point for the older populations just a few percent.

Morphological and spectral gradients similar to this are seen in low- $z$  clusters (e.g. Oemler, 1974; Dressler, 1980; Whitmore et al., 1993). Similar gradients over large scales at higher redshifts have also been noted by Abraham et al., (1996), Couch et al., (1998) and Dressler et al., (1997). Balogh et al., (1997) traced the star formation gradients in this CNOC sample via measurements of the [OII] emission line and also found a similar trend. Such gradients are consistent with the infall of field galaxies in hierarchical clustering models of cluster growth (e.g. Gunn & Gott, 1972; Kauffmann et al., 1995a,b) and suggest that galaxies which have more recently fallen into the cluster potential preferentially inhabit its outskirts.

The PCA components can be transformed to measure a galaxy's match to any specific stellar population. In Figure 4 we plot a weighted composite for the sample, where the components are redefined. “Cluster” values were chosen to match ellipticals in the Kennicutt Atlas (1992), and agree with the reddest galaxies in these clusters. Spectral synthesis models (Charlot & Bruzual, 1993) indicate that any population more than about 3 Gyr old will yield similar PCA values. The new “Field-like” vector is calculated separately for each cluster, based on the average for field galaxies at these same magnitudes at the cluster redshift from the CNOC2 Field Redshift Survey (Carlberg et al., 1998). On average, values are similar to a present-day Sbc, but with additional power in

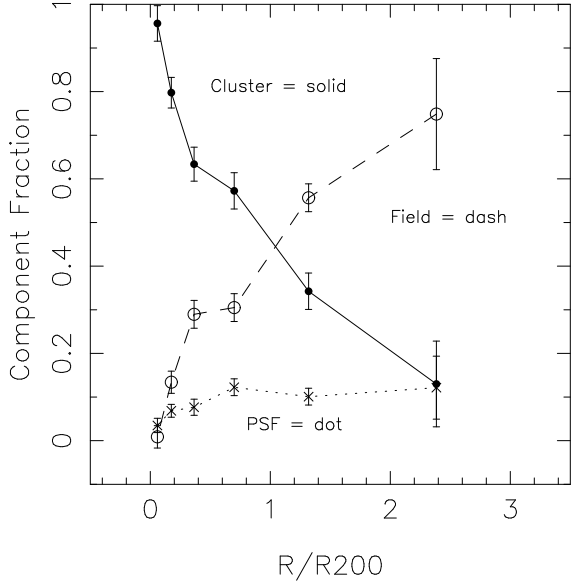


Figure 4. Composite radial gradients in transformed coordinates (see text).

Balmer absorption lines. There is a mild increase in the “Emission” fraction between  $z=0.2$  and  $z=0.6$ . “Post-Star-Formation (PSF)” values are determined from a spectral synthesis model of a galaxy whose star formation is constant for 4 Gyr and then is abruptly stopped. The new vector corresponds to the time of the maximum Balmer component, about 0.5 Gyr after the truncation, and is in general agreement with PCA values from the strong K+A spectra of galaxies seen in the clusters.

Note that these components are not strictly orthonormal, though they are normalized to a sum of unity, as before. Thus, the equivalent of total flux is conserved, but the component values are dependent on the choice of all three vectors. While the “Cluster” and “Field-like” components are robustly determined empirically, the “PSF” component is more arbitrarily defined. Choosing a slightly different recipe for this component will raise or lower all three values slightly.

Despite this potential degeneracy, the overall cluster structure is well illustrated by this transformation. Old population galaxies preferentially occupy the cluster interior, and a smooth gradient towards younger populations is seen until the properties of cluster galaxies (defined from their redshifts) asymptotically approach those of the coeval field population at  $2-5 r_{200}$ , well outside of the virial radius.

The post-star-formation component appears relatively flat, with a component fraction of about 10%. This is larger than the fraction of identifiable K+A galaxies seen in the same dataset by Balogh et al., (1999), but smaller than the fractions seen by Poggianti et al., (1999) in the MORPHS sample of clusters at similar redshifts. The PCA technique, of course, is sensitive to smaller fractions

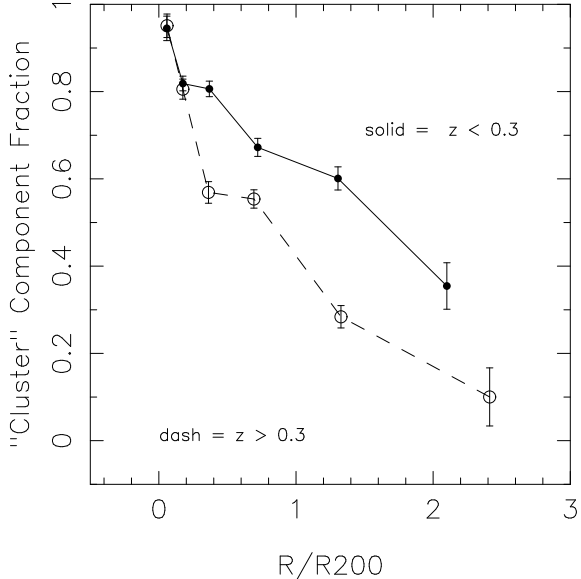


Figure 5. Composite radial gradients in the “Cluster” component as a function of cluster redshift.

of galaxy light in the post star formation state, so higher fractions are expected than for studies which count only galaxies with extreme signatures. Thus the comparison with Balogh et al., appears reasonable. However, the comparison with the MORPHS clusters is more troubling, and may signify true differences in cluster populations for X-ray selected clusters such as the EMSS sample, versus the optically selected MORPHS clusters. One possibility is that the former sample is likely to be more relaxed and centrally concentrated, whereas optically selected clusters may include objects with more recent infalling structures, which may explain a higher fraction of galaxies which have recently had their star formation truncated.

In Figure 5 we examine the trend in population gradients in clusters over our redshift range of 0.18 to 0.55. Plotted are the “Cluster” components versus radius for samples at  $0.18 < z < 0.3$  and  $0.3 < z < 0.55$ . The PCA values, weights and uncertainties are calculated as before. While the cluster cores appear to be similarly dominated by old populations, a significant change in the cluster gradient is seen between the two redshift bins. At lower redshift, the old population appears to dominate to larger radii, whereas at high redshifts, the field galaxies are more noticeable in the inner portions of the cluster. This steepening of the population gradient can be thought of as a more detailed restatement of the Butcher-Oemler effect, which describes the increasing blue fraction in higher redshift clusters, typically measured inside of  $0.5 h^{-1}$  Mpc.

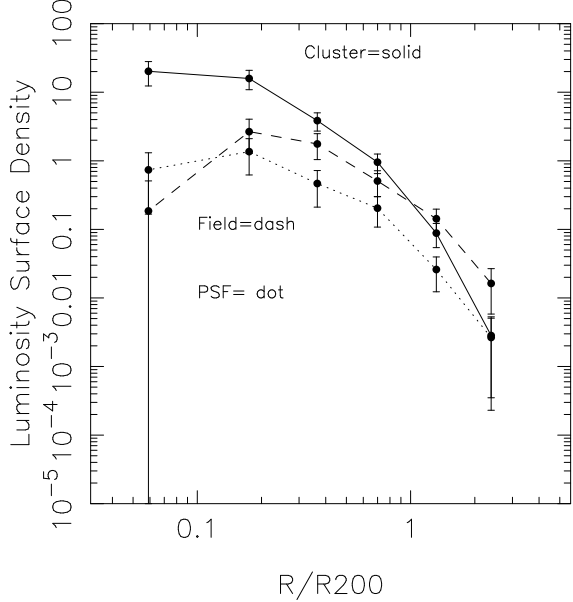


Figure 6. Composite luminosity density profiles from 15 clusters based on the transformed vector coordinates. The profiles show an increasing spatial extent from “Cluster” to “Post-Star-Formation” to “Field-like.”

### 5. Luminosity Density Profiles

From the principal component analysis, relative luminosity surface density profiles can also be constructed, to trace the total light associated with the various stellar populations. Figure 6 shows the profiles for the transformed vector coordinates described above. The fractional gradients seen in Figures 3 and 4 are shown here to be caused by light distributions which increase in extent from older to younger. This is quite consistent with what is expected from the accretion of field galaxies into the cluster. At first, infalling galaxies should have a relatively flat distribution, and as the galaxies become dynamically incorporated into the cluster, their distribution will appear more virialized, with a tighter profile. This dynamical evolution occurs in tandem with spectral evolution, causing the observed population gradients.

In Figure 7 we illustrate a possible explanation for the evolution in cluster populations and population gradients in clusters by constructing luminosity profiles as a function of cluster redshift. Figure 7a shows the relative luminosity surface density for the old “Cluster” component for  $0.18 < z < 0.3$  and  $0.3 < z < 0.55$ . The two curves are normalized to have the same total number of galaxies with  $0.5 \text{ h}^{-1} \text{ Mpc}$  in both bins. It appears that the old population has not changed in shape significantly over this timescale, which is in agreement with the idea that these galaxies are in a stable dynamical equilibrium. This population contains light both from any elliptical galaxies which may have formed early in the cluster history, as well as once star forming galaxies which have had their star formation truncated 3 Gyr or more ago.

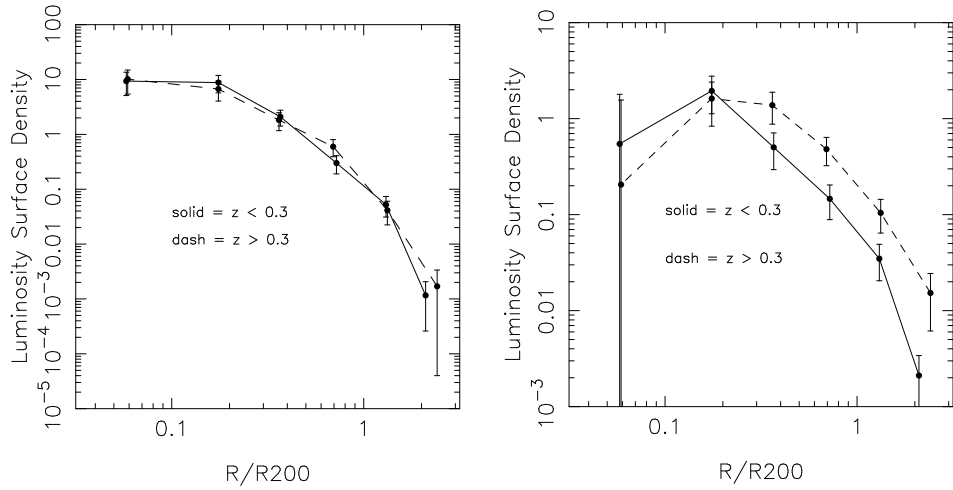


Figure 7. Composite luminosity density profiles from 15 clusters as a function of redshift. Figure 7a (left) shows profiles for the “Cluster” component for clusters with  $0.18 < z < 0.30$  (solid) and  $0.30 < z < 0.55$  (dash). Figure 7b (right) shows the profiles for the sum of the “Field-like” and “PSF” components and the same redshift bins.

Figure 7b shows the sum of the “Field-like” and “Post-Star-Formation” light profiles, representing galaxies which are newer introductions to the cluster potential. These curves are normalized identically to those in Figure 7a. Here the Butcher-Oemler effect is again obvious, with a higher density of younger populations being seen at higher redshifts. Outside the core region ( $> 0.25 r_{200}$ ) these curves also appear to be similar in shape, suggesting that dynamical state (i.e. time since entry to the cluster potential) and age of the stellar populations are fundamentally linked. This is a reasonable assumption if the mechanism which transformed the population is due to the cluster environment. The main difference in these curves is then a simple vertical shift, and these results can thus be interpreted as a decline in the infall rate of new galaxies into the cluster.

Linking this interpretation to cosmological models remains uncertain because of the unknown timescales of both virialization and population evolution in these environments. For example, the mechanism which affects ongoing star formation in clusters may operate quite gradually, and the “field” galaxies we see in the cluster may have been introduced to the cluster a billion or more years earlier than the observed epoch. The observed epochs are at  $z \sim 0.23$  and  $z \sim 0.43$ ; a rough estimate of at least 1 billion year delay between infall and the start of the spectral transformation would place the epoch of maximal infall into clusters at  $z > 0.7$ , in agreement with predictions from a low-density universe.

## 6. Other Scenarios for Galaxy Evolution in Clusters

An alternate viewpoint to a declining infall rate is that some physical property of the cluster environs has evolved over these timescales, driving the observed

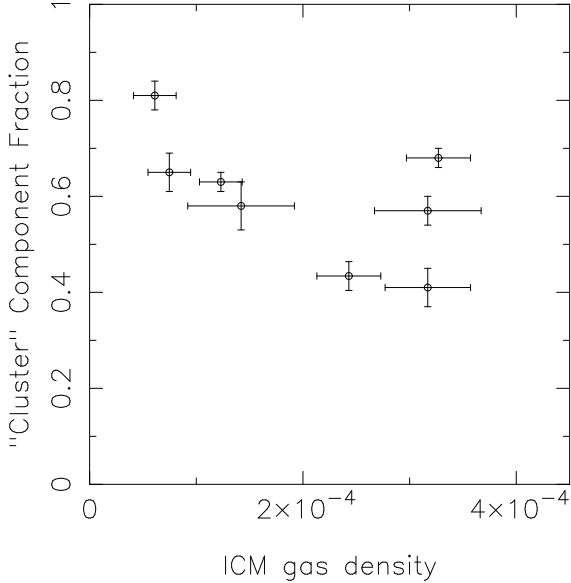


Figure 8. “Cluster” component value versus X-ray gas density, (units of  $\text{cm}^{-3}$ ) as measured at  $0.5 r_{200}$ . direct link between cluster population evolution and X-ray gas evolution would predict a positive correlation. None is seen, suggesting that other factors drive the observed evolution.

evolution in the populations. Possibilities include evolution of the infalling field population, differing rates or efficiencies of galaxy-galaxy interactions, and evolving gas densities in the cluster, which would affect the efficiency of ram-pressure stripping of gas from infalling galaxies. We have essentially removed the effects of field galaxy evolution by constructing vector components which are based on the observed field population at the same magnitudes and redshifts as the clusters.

Global evolution in the X-ray gas is also probably not a strong driving force in the observed evolution. All of the clusters in our sample are luminous X-ray clusters, and there does not appear to be a strong correlation between the X-ray gas and the galaxy populations. Figure 8 shows the old “Cluster” component for 8 clusters versus azimuthally averaged X-ray gas density, each measured at  $0.5 r_{200}$  from the cluster core. While there is some variation in each parameter, they do not appear positively correlated, as would be expected if gas density evolution were driving the overall population changes. (Note that gas stripping may still be responsible for the transformation of individual galaxies, while a cosmologically changing condition drives the population evolution.)

Another possibility is that at higher redshift, infalling galaxies have a larger reservoir of interstellar gas, and hence are more resilient to stripping. If this were the case, we would expect to see that the “Field-like” population would have a tighter, more evolved spatial distribution at higher redshift than at lower redshifts. Figure 7 cannot quantitatively rule out this possibility; however the data

appear to be more consistent with the distributions keeping the same shape, with a simple vertical shift, rather than the higher redshift distributions having a higher peak towards the inner regions due to a dynamically relaxed but spectroscopically unevolved population.

Galaxy-galaxy interactions remain a possible mechanism for galaxy evolution in clusters, although morphological evidence for this remains mixed (e.g. Oemler et al., 1997). Since the effects of cluster richness and dynamics are normalized in this analysis, any evolutionary effect must come from either a cosmological change in the clustering of galaxies as they fall into the cluster (i.e. a declining rate of infalling pairs or small groups which might preferentially inhabit the regions near clusters), or in the resiliency of galaxies at continuing to form stars in the wake of a collision.

## 7. Conclusions

We have carried out a principal component analysis of galaxies in 15 clusters at intermediate redshift to investigate the relationship between cluster population and global spatial/dynamical structure. Composite population gradients show a smooth transition from the infalling field galaxy population to the older populations seen in the cluster core. The gradients are corrected for the evolution of the field population and cluster richness. Evolution between  $z=0.6$  and 0.2 is manifest in a flattening of this gradient at later epochs, consistent with the Butcher-Oemler effect. This phenomenon is most consistent with scenarios where the mechanism which truncates star formation in individual galaxies remains constant, but the cluster population evolution is driven by a declining rate of infall into the clusters. Scenarios in which galaxies at earlier times are more resilient to destructive environmental effects of the cluster may also be possible.

**Acknowledgments.** EE acknowledges support provided by the National Science Foundation grant AST 9617145. HL acknowledges support provided by NASA through Hubble Fellowship grant #HF-01110.01-98A awarded by the Space Telescope Science Institute, which is operated by the Association of Universities for Research in Astronomy, Inc., for NASA under contract NAS 5-26555.

## References

- Abraham, R. G. et al., 1996, ApJ, 471, 694
- Barger, A. et al., 1998, ApJ, 501, 522
- Balogh et al., 1997, ApJ, 488, L75
- Balogh et al., 1999, in press
- Bower, R. G., Lucey., J. R., & Ellis, R. S., 1992, MNRAS, 254, 601
- Butcher, H., & Oemler, A. 1984, ApJ, 285, 426
- Carlberg et al., 1996, ApJ, 462, 32
- Carlberg et al., 1997a, ApJ, 476, L7
- Carlberg et al., 1997b ApJ, 479, L19
- Carlberg, R. et al. 1998, astro-ph/9805131

Carlberg, R. G., Yee, H. K. C., & Ellingson, E. 1997, *ApJ*, 478, 462  
Charlot, S. & Bruzual G. 1993, *ApJ*, 405, 538  
Coleman, G.D., Wu, C.C., & Weedman, D.W. 1980, *ApJS*, 43, 393  
Connolly et al., 1995, *AJ*, 110, 1071  
Couch et al., 1998, *ApJ*, 497, 188  
Dressler, A. 1980, *ApJ*, 236, 351  
Dressler, A., 1997, *ApJ*, 490, 577  
Ellis, R. et al., 1997, *ApJ*, 483, 582  
Gunn, J. E., & Gott, J. R. 1972, *ApJ*, 176  
Kauffmann, G. 1995a, *MNRAS*, 274, 153  
Kauffmann, G. 1995b, *MNRAS*, 274, 161  
Kennicutt, R. 1992, *ApJS*, 79, 255  
Lewis et al., 1999, *ApJ*, 517, 587  
Oemler, A. 1974, *ApJ*, 194  
Poggianti, B. et al., 1999, *ApJ*, 518, 576  
Richstone, D., Loeb, & Turner, E. L. 1992, *ApJ*, 393, 477  
Whitmore, B. C., Gilmore, D. M., & Jones, C. 1993, *ApJ*, 407, 489  
Yee, H. K. C., Ellingson, E., & Carlberg, R. G. 1996, *ApJS*, 102, 269  
Zaritsky, D., Zabludoff, A. I., & Willick, J. A., 1995, *AJ*, 110, 1602